Molecular Therapy
Methods & Clinical Development
Original Article

Near-Infrared Laser-Based Spatially Targeted Nano-enhanced Optical Delivery of Therapeutic Genes to Degenerated Retina

Subrata Batabyal,[1] Sivakumar Gajjeraman,[1] Kissaou Tchedre,[1] Adnan Dibas,[1] Weldon Wright,[1] and Samarendra Mohanty[1]

[1]Nanoscope Technologies, 1312 Brown Trail, Bedford, TX 76022, USA

Non-viral delivery of therapeutic genes into targeted areas of retina is essential for re-functionalizing the retinal circuitry. While a focused ultrafast laser beam has been recently used for intra-ocular delivery of molecules, it poses the significant technical challenge of overcoming aberrations of the eye and maintaining a tightly focused spot on the retinal cell membrane. Furthermore, to minimize collateral damage and increase the throughput of gene delivery, we introduced a weakly focused near-infrared (NIR) continuous wave (CW) or pulsed laser beam on to the cells wherein the intensity is locally enhanced by gold nanorods bound to the cell membranes to permit gene insertion. Parametric optimization of nano-enhanced optical delivery (NOD) was carried out by varying the exposure time, as well as the power of the CW NIR beam or the energy of the pulsed NIR beam. Using this NOD method, therapeutic genes encoding for multi-characteristic opsins (MCOs) were delivered to spatially targeted regions of degenerated retina *ex vivo* as well as *in vivo*. NOD-mediated cell membrane-specific expression of MCOs in targeted retinal regions with photoreceptor degeneration will allow functional recovery in an ambient light environment.

INTRODUCTION

Gene therapy is emerging as a powerful approach with the potential to treat and even cure some of the most common diseases. Somatic gene therapy[1,2] requires delivery of genomic materials[3] into specific cells of the targeted organ. Targets of gene therapy include varieties of inherited diseases, including central nervous system disorders such as retinal degenerative diseases and acquired diseases in the heart, lung, and blood. Recently, opto-gene[4–9] therapies based on precise optical modulation[10–13] of the nervous system are receiving significant attention for treatment of several neurological[14–20] and retinal disorders. Opto-gene therapies of retinal degenerative diseases such as dry age-related macular degeneration (dry-AMD) require photosensitization of higher order retinal neurons. Gene delivery by commonly used viral transfection[21–23] can lead to unexpected immunological, inflammatory responses and limit the size of the packaged genes that can be delivered.[2,24] Significant efforts have been made for the development of non-viral gene delivery vehicles, including physical (microinjection,[25] gene gun, electroporation,[26,27] ultrasound,[28] hydrodynamics, magnetofection) and chemical (liposomes,[29] biodegradable polymer nanoparticles[30]) methods to allow delivery of large macromolecules. However, these methods have reduced transfection efficiency as well as adverse effects on non-targeted cells.[26] While viral and other delivery methods can achieve cell-specific targeting by either tropism of viral vectors or promoter-driven expression, most of the existing methods cannot achieve spatially targeted transfection to localize the expression (among identical cell types) in the organ of interest. A recently developed method has shown use of a functionalized glass pipette tip or magnetic nanoparticles in a pipette bound to the virus for contact-based "virus stamping" on the target cell using mechanical or magnetic forces.[31] Spatially targeted non-contact and minimally invasive gene delivery is of special importance for clinical translation of current optogenetic approaches for treatment of geographic atrophic regions of the degenerated retina[32–36] without perturbing the functioning of the non-degenerated retinal regions.

In our earlier work,[37] we demonstrated non-contact single-cell transfection of opsin *in vitro* using a focused ultrafast laser beam. However, use of such an approach for optoporation requires matching the focal plane with the cell membrane in order to create transient perforation and therefore may require aberration corrections via adaptive optics. Furthermore, parallel transfection of cells in spatially targeted regions using such a method will require use of multiple beams, which will be limited by the damage threshold of the spatial light modulator. This necessitates development of a high-throughput, easily applicable method for gene delivery to spatially targeted regions of tissue in a minimally invasive manner.

Herein, we report on the use of nano-enhanced optical delivery (NOD) of plasmids encoding ambient light-sensitive multi-characteristic opsin[38] (MCO-II) into spatially targeted retina *ex vivo* as well as *in vivo* in a mice model of retinal degeneration using a near-infrared (NIR) (1,064 nm) laser beam. The optical field of the defocused NIR

Received 15 March 2020; accepted 30 March 2020;
https://doi.org/10.1016/j.omtm.2020.03.030.

Correspondence: Samarendra Mohanty, Nanoscope Technologies, 1312 Brown Trail, Bedford, TX 76022, USA.
E-mail: smohanty@nanoscopetech.com

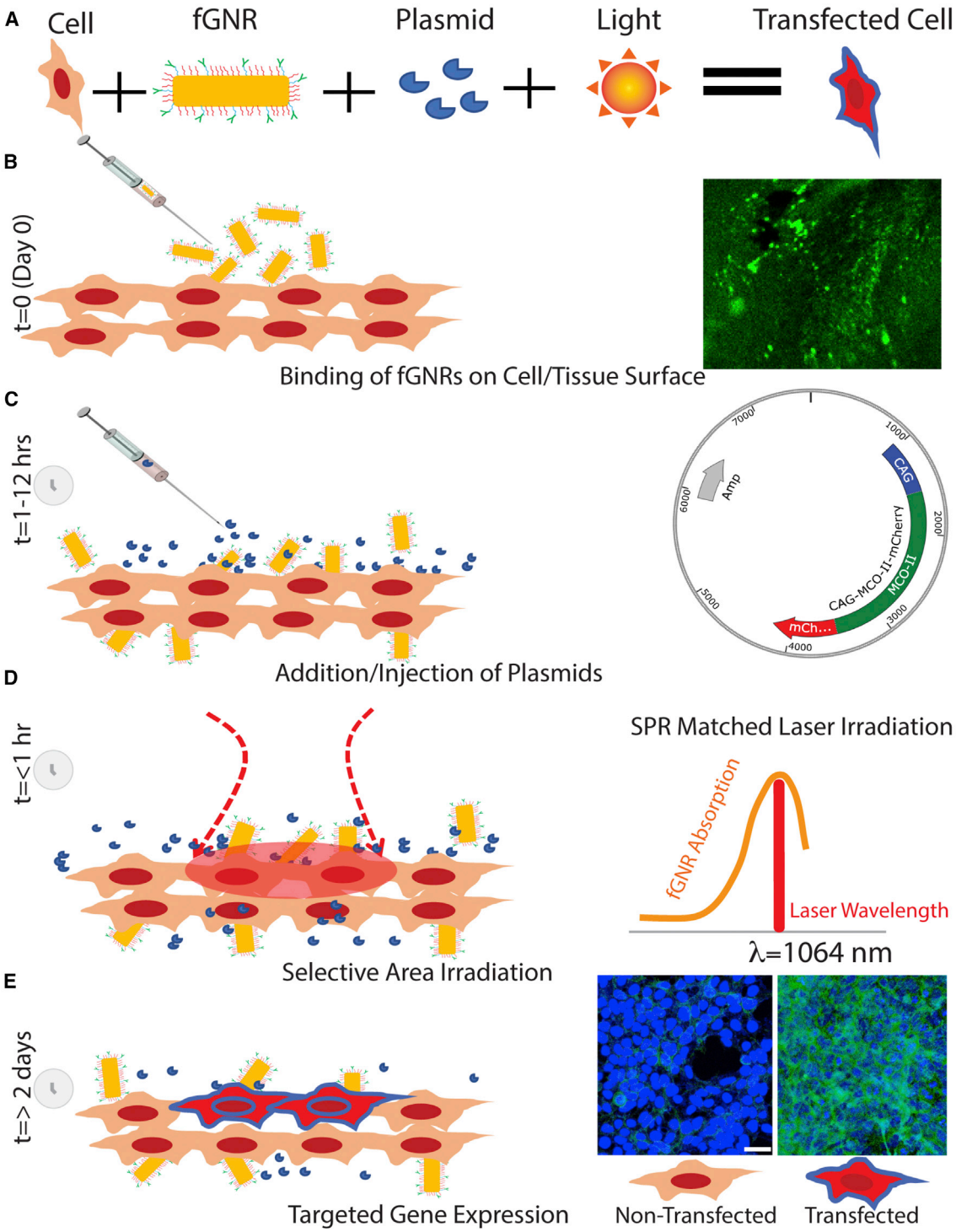

Figure 1. Method of Nano-Enhanced Optical Delivery (NOD)

Upon illumination of a laser beam of a specific wavelength, the functionalized gold nanorods (fGNRs) generate localized membrane permeabilization, allowing insertion of genes into the cells in the targeted areas. (A) Components involved in NOD. (B–E) Sequential steps of the spatially targeted NOD. (B) Addition of fGNRs onto cells/tissues.

(legend continued on next page)

laser beam was enhanced by surface plasmon resonance (SPR) at the metal (gold nanorod [GNR])-dielectric (cell) interfaces, allowing insertion of large MCO-II genes in the illuminated region in a high-throughput manner, without affecting the non-targeted tissues. Parametric studies of NOD carried out by varying the exposure time and power of the continuous wave (CW) NIR beam or the energy of the pulsed NIR beam led to determination of optimized parameters for gene delivery. Successful translation of NOD will enable spatially targeted, cell-specific gene therapy for a multitude of disorders of the central and peripheral nervous systems.

RESULTS

Mechanism and Steps Involved in NOD

Figure 1 depicts the components and various steps involved in the NOD of therapeutic genes to specific groups of cells. In this NOD approach, GNRs are functionalized with concanavalin A (Con A) (functionalized GNRs [fGNRs]) to facilitate their binding to the membrane of the cells (Figure 1B). Figure S1 shows a transmission electron microscopy (TEM) image of GNRs used for optical enhancement of a 1,064-nm laser beam (hotspots) at the ends of the rods. Figure S1B shows measured optical density of GNRs with a peak at 1,064 nm. The inset in Figure 1B shows fluorescently labeled fGNRs bound to cells. After 1–12 h of incubation with fGNRs, the therapeutic (MCO) plasmids (vector map in inset of Figure 1C) are introduced onto the cells. Next, the NIR laser beam wavelength, tuned to the SPR peak of the fGNRs (inset in Figure 1D), is applied onto targeted areas as shown in Figure 1D. Due to SPR-matched absorption of the NIR laser irradiation, hotspots at the ends of the nanorods are generated. The contrast in the temperature increase in laser-irradiated nanorod-attached cell membranes near the hotspots is significant enough for permeabilization of the cell membrane, leading to site-specific intra-cellular delivery of impermeable molecules from the extra-cellular space.[39,40] Figure 1E (inset) shows representative non-transfected and transfected cells in the laser-targeted area 2 days after NOD.

Nanosecond NIR Laser-Assisted NOD Enabled Membrane-Localized MCO-II Gene Expression in Human Embryonic Kidney (HEK) Cells

To demonstrate the ability of NOD (+ plasmids, + fGNRs, and + 1,064-nm laser) for delivery of large therapeutic genes such as MCO-II, a nanosecond-pulsed laser (1,064 nm) beam was used for transfection into the HEK cells. The immunostained image in Figure 2A shows nanosecond-pulsed laser (10 mJ, 10 Hz)-based NOD of MCO-II-mCherry into HEK cells in a Petri dish using a total laser dose of 5 mJ/mm^2 (10 mJ/pulse, 10 Hz, 10 s, 200-mm^2 area). Figure 2B (3× zoomed image of the square region marked in Figure 2A) shows robust expression of the reporter mCherry. The absence of fluorescence in the staining control (− primary antibody, + secondary antibody), as well as the 3× zoomed images of NOD regions (Figures 2C and 2D), confirms the presence of mCherry. The distribution of the reporter protein along the cell was quantified by plotting the intensity level along lines drawn across the cells (Figure 2E). The expression level in membrane and intracellular regions was quantified based on reporter intensity as shown in Figure 2F. Higher membrane-specific expression can be observed in cells after NOD of MCO-II-mCherry plasmids. Cells in non-targeted (without NOD laser) regions with or without plasmids and fGNRs did not show reporter fluorescence, as illustrated in confocal images (Figures S2A–S2D). Quantitative comparison of mCherry expression in NOD-treated and control cells is shown in Figure 2G. To optimize NOD-based transfection of MCO-II into HEK cells using a 1,064-nm nanosecond laser beam, the energy/pulse was varied from 10 to 30 mJ, resulting in an energy density of 2.5–15 mJ/mm^2 (spot size, 200 mm^2). Two different exposures (5 and 10 s) were used for each energy pulse. The transfection efficiency (measured as the number of fluorescent cells/total cells) at different NOD laser beam parameters (i.e., energy pulse and exposure time) is shown in Figure 2H. Figure S3 shows nuclear (DAPI, blue)- and mCherry (green)-immunostained images of HEK cells transfected by the nanosecond NIR laser beam at different irradiation parameters.

Ex Vivo Transfection of a Retinal Explant Using Nanosecond NIR Laser-Based NOD Led to Robust Expression

To demonstrate NOD into retinal cells, *rd10* mouse (retinal degeneration 10, spontaneous missense point mutation in Pde6b)) retinal explants were used. Figure 3 shows the nanosecond-pulsed NIR (1,064 nm) laser beam-based spatially targeted parallel transfection of MCO-II-mCherry in retinal explants. No cellular expression in the retina explants in the absence of a NOD laser beam-was observed (Figure 3A). Using a 1,064-nm laser beam (dose, 5 mJ/mm^2), NOD was then carried out in explants. The immunostained retinal explants showed robust expression of MCO-II mCherry in the targeted areas (Figure 3B) as compared to the non-targeted control (Figure 3A). To quantify the relative expression of mCherry in the cell membrane and intracellular components, intensity profiles along a line drawn across the image of immunostained cells (Figure S4A) were plotted (Figure S4B). The MCO-II expression in plasma membrane was found to be significantly higher than intracellular expression (Figure S4C). A comparison of MCO-II-mCherry expression (measured by average mCherry fluorescence intensity) in targeted versus non-targeted regions in retina explant is shown in Figure 3C. No detectable increase in fluorescence in the mCherry emission band was observed in non-laser-exposed explants incubated with GNRs and MCO-II-mCherry plasmids.

To measure intensity-dependent MCO-II delivery and expression by NOD, the retina explant was irradiated with a Gaussian beam with varying intensity (decreasing from the center). A confocal fluorescence image of an immunostained retina explant (Figure 3D) shows distribution of reporter (mCherry) expression in a targeted area

Inset: fluorescently labeled fGNRs bound to cells. (C) Introduction of therapeutic (MCO) plasmids onto the cells after 1–12 h of incubation with fGNRs. Inset: vector map of MCO-II-mCherry plasmid. (D) Laser irradiation of targeted area within 1 h of introduction of plasmids. Inset: laser irradiation wavelength (1,064 nm) matching to surface plasmon resonance (SPR) of fGNRs. (E) Evaluation of gene expression in targeted cells/tissues >2 days after NOD. Inset: representative non-transfected and transfected cells.

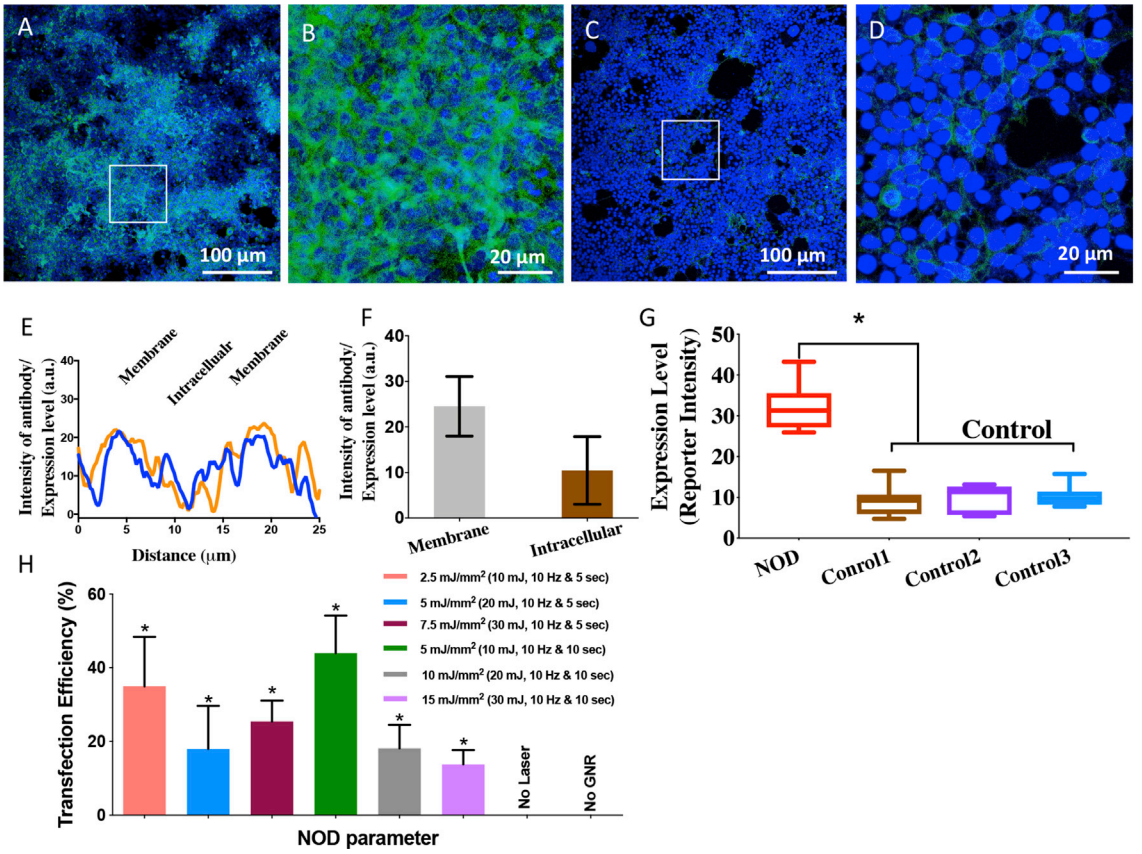

Figure 2. Nanosecond-Pulsed Laser Beam-Based NOD Achieved High-Throughput Transfection of MCO-II-mCherry Plasmids in HEK Cells

(A) Immunostained fluorescence image of HEK cells in a Petri dish transfected with MCO-II-mCherry using NOD (+ plasmids, + fGNRs, + 1,064-nm laser) using total laser dose of 5 mJ/mm^2 (10 mJ/pulse, 10 Hz, 10 s, 200-mm^2 area). (B) Zoomed image of the region marked by the square in (A). (C) Immunostained fluorescence image of staining control. (D) ×3 zoomed image of the region marked by the square in (C). (E) Plot of fluorescence intensity of reporter (mCherry) along a line drawn across the transfected cell, showing membrane-specific expression. (F) Quantitative comparison of reporter fluorescence in membrane and cytoplasm. (G) Quantitative comparison of mCherry expression in NOD-transfected cells and controls: (1) − plasmid, − fGNRs, − 1,064-nm laser; (2) − primary antibody; and (3) − 1,064-nm Laser. Primary antibody, anti-mCherry; secondary antibody, Alexa Fluor 488 (green). Nuclear staining with DAPI (blue). Mean ± SD. (H) Transfection efficiency (measured as number of fluorescent cells/total cells) at different NOD laser beam parameters (i.e., energy/pulse and exposure time), with total dose ranging from 2.5 to 15 mJ/mm^2. *$p < 0.05$ with respect to the "no laser" and "no fGNRs" controls. Mean ± SD.

irradiated with an elliptic nanosecond-pulsed laser beam in the presence of fGNRs and MCO-II-mCherry plasmids. The radial distribution profile of expression along the x and y axes in the retinal explant (Figure 3E) follows the Gaussian irradiation beam. Figure 3F shows transfection efficiency (measured by the percentage of fluorescence-positive cells) as a function of distance from the center of the NOD laser beam. Based on these *ex vivo* studies, the optimal laser parameters for NOD were determined to be 0.5 mW/mm^2 (average power density) and 10-s exposure for an ns laser (10 mJ/pulse, 10 Hz), resulting in a dose of 5 mJ/mm^2.

CW NIR Laser-Assisted *In Vitro* NOD Enabled MCO-II Gene Expression

To examine whether a CW NIR laser beam can achieve NOD and to determine the laser dose, *in vitro* experiments were performed for delivery of MCO-II-mCherry plasmids into HEK293 cells. The cells were exposed to two different laser powers (80 and 120 mW) and two different durations (30 and 60 s), leading to a total dose of 600–1,800 mJ/mm^2 (spot size, 2 mm). There is no cellular expression in retina explants in the absence of an NOD laser beam (control; + plasmids, + fGNRs, − 1,064-nm laser), as shown in Figure 4A. Some non-specific binding of secondary antibodies was observed, but it exhibited very low fluorescence intensity. The reporter (mCherry) expression is evident in cells in the NOD-targeted area (Figure 4B) imaged 2 days after NOD. The 1,064-nm NOD-based MCO-II delivery efficiency at different laser doses was quantified based on the measured mCherry (reporter)-bound antibody fluorescence intensity of cells (averaged) in targeted areas. Figure 4C shows the variation of expression level as function of four different laser doses. The NOD-transfected cells showed membrane-specific expression of the MCO-II reporter as shown in intensity profiles (Figure 4D) along lines drawn across the transfected cells. Quantitative

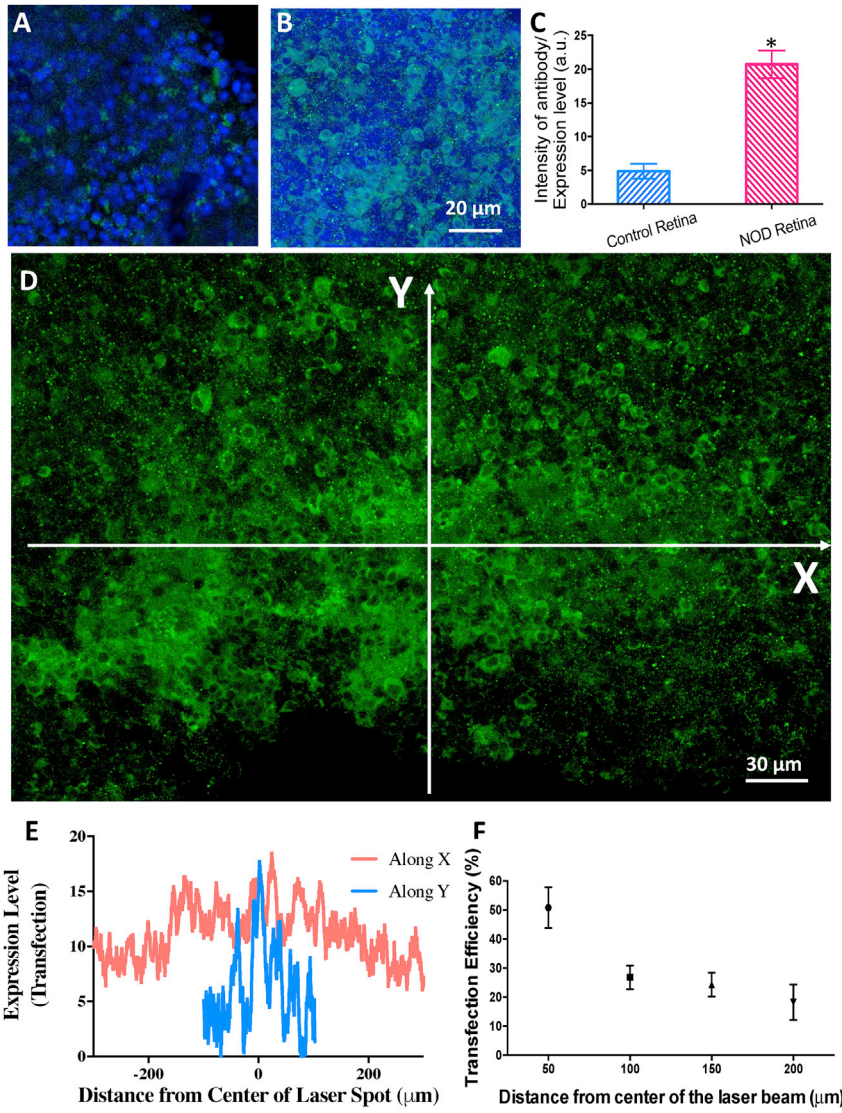

Figure 3. Spatially Targeted Parallel Transfection of MCO-II-mCherry into Retinal Cells in Explants Using Nanosecond-Pulsed Laser Beam-Based NOD

(A) No cellular expression in the retina explants in the absence of an NOD laser beam (i.e., + plasmids, + fGNRs, – 1,064-nm laser). (B) Fluorescence image of retinal explant, showing cellular expression of MCO-II mCherry (immunostained) upon NOD (1,064-nm laser dose, 5 mJ/mm^2). (C) Quantitative comparison of mCherry expression (measured by fluorescence intensity) in NOD-transfected and control retina. *$p < 0.01$. Mean ± SD. (D) Representative fluorescence image of immunostained retina explant, showing the distribution of reporter (mCherry) expression in a targeted area irradiated with an elliptic nanosecond-pulsed laser beam in the presence of fGNRs and MCO-II-mCherry plasmids. (E) Radial distribution profile of expression along the x and y axes in the retinal explant follows the Gaussian irradiation beam. (F) Transfection efficiency (measured by percentage of fluorescence-positive cells) as a function of distance from the center of the NOD laser beam. Mean ± SD.

comparison of mCherry expression in membrane versus intracellular compartments is shown in Figure 4E.

Figure 4F shows the measured transfection efficiency (percentage of fluorescent cells) at different NOD laser beam doses (power × exposure time) ranging from 600 to 1,800 mJ/mm^2. Western blot was performed to confirm the MCO expression in HEK cells transfected by NOD or the standard (lipofection) method. Figure 4G shows the chemiluminescence western blot of immunoprecipitated MCO-II-mCherry (894 residues) from cells transfected by NOD along with that from cells transfected by lipofection (positive control). The MCO-II-mCherry protein band was detected at ~200 kDa, which is approximately double that of the molecular mass (~100 kDa) calculated from the translation of the transgene sequence. The dimeric form of the *in vitro* MCO-II-mCherry protein predominantly gave the higher molecular mass band in western blot. For the same number of total cells exposed to the same amount of plasmids and transfection reagent (i.e., lipofection or laser and GNRs), the MCO-II-mCherry expression (quantified by the intensity and area of the specific chemiluminescence band) in cells transfected by NOD was comparable to that in cells transfected by lipofection.

CW NIR Laser-Assisted NOD Led to MCO-II Gene Expression *In Vivo*

After the successful *in vitro* NOD experimental results in *rd10* mice retina explants, *in vivo* transfection of MCO-II opsin plasmids into the retina of *rd10* mice was carried out. Figure 5A shows the schematic representation of *in vivo* NOD in a mouse eye and the subsequent steps to visualize the expression. NOD using a 1,064-nm CW laser beam was carried out with the *in vivo* setup built on a surgical microscope (Figure S5A). To confirm binding of GNRs (with the SPR peak at 1,064 nm) to retina (an essential step for NOD), we injected fluorescently labeled (Alexa Fluor 488 carboxylic acid, succinimidyl ester) fGNRs (1 μL) intravitreally to mouse eyes. Fluorescence images of retina after intravitreal injection of fluorescence (Alexa Fluor 488) dye and control (no dye injection) are shown in Figures 5B and 5C, respectively. The confocal fluorescence image of retina extracted ~1 h after intravitreal injection of fluorescence dye-labeled fGNRs shows distinct florescence speckles indicative of fGNR binding on retina (Figure 5D). To evaluate the presence of fGNRs in retina during a longer period, the retinas were extracted 12 h (overnight) after intravitreal injection of fluorescently tagged fGNRs. Fluorescence images after overnight incubation (in the eye) are shown in Figure 5E. The binding of Con A-conjugated GNRs (injected intravitreally) was found to last at least 12 h in the retina.

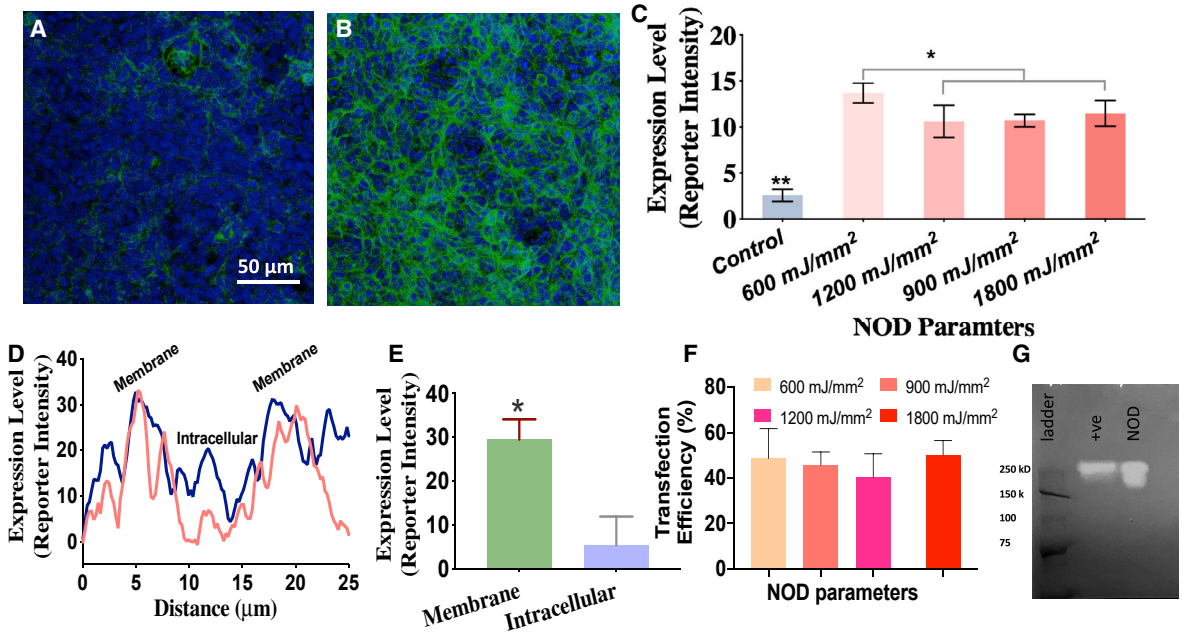

Figure 4. Continuous Wave near-infrared laser based parametric evaluation of NOD for *in vitro* transfection of MCO-II-mCherry plasmids in HEK cells.
(A) No cellular expression in the cells in the absence of a NOD laser beam (i.e., + plasmids, + fGNRs, − 1,064-nm laser). (B) Fluorescence image of cells, in NOD-targeted area in Petri dish, immunostained with mCherry antibody (green) and DAPI (blue). (C) Quantification of expression (measured by fluorescence intensity) in cells for different NOD parameters (total laser doses of 600, 900, 1,200, and 1,800 mJ/mm^2 with laser spot size of ~2 mm). Mean ± SD. *$p < 0.05$ between 600 mJ/mm^2 and others; **$p < 0.01$ between control and others. (D) Plot of fluorescence intensity of reporter (mCherry) along a line drawn across the transfected cells, showing membrane-specific expression. (E) Quantitative comparison of mCherry expression in membrane versus intracellular regions of NOD-transfected cells. *$p < 0.05$. (F) Transfection efficiency (measured as percentage of fluorescent cells) at different NOD laser beam doses (power × exposure time) ranging from 600 to 1,800 mJ/mm^2. Mean ± SD. (G) Chemiluminescent western blot of lysates of HEK cells transfected with MCO-II-mCherry by NOD or by commercially available transfection reagents (transfection by jetPRIME: positive control) showing the MCO-II-mCherry expression level.

For conducting NOD, 1 h after injection of 1 µL of Con A-functionalized GNRs (inside eye concentration, 30 ng/µL), 1 µL of MCO-II-mCherry plasmid solution was injected intravitreally into an *rd10* mouse eye to result in a final concentration of 500 ng/µL plasmid inside the eye. To allow CW NOD laser beam irradiation of retina, the mouse eye was dilated with tropicamide (Figure S5B). After dilation, the CW NIR laser beam was applied for 30 s on the retina. Figure S5C shows an image of mouse retina being irradiated by the NIR NOD laser beam with a dose of 600 mJ/mm^2 (20 mW for 30 s, 1-mm^2 area). Figure 5F is an immunostained confocal image of a NOD-treated *rd10* mouse eye, showing expression of MCO-II-mCherry (red) in the targeted area of retina. The cellular expression was confirmed by higher resolution confocal fluorescence imaging of the mCherry-immunostained retina overlaid on nuclear stain (Figures 5G and 5H).

Figure 5I shows the chemiluminescence western blot of immunoprecipitated MCO-II-mCherry (894 residues) from cells transfected by NOD along with that from retinal cells transfected *in vivo*. The retina was freshly harvested and lysed in radioimmunoprecipitation assay (RIPA) buffer. The concentration of the total extracted protein was found to be 0.5 µg/µL. 75 µg of the total protein was subjected to immunoprecipitation, and the whole immunoprecipitated sample was subjected to western blot. The MCO-II-mCherry protein band was detected at ~90 kDa, which matches with the theoretically calculated molecular mass from the translation of the transgene sequence.

To evaluate gene expression for different fGNR-incubation periods, we used two laser powers (60 and 120 mW) and an exposure duration of 30 s, resulting in total dose of 1.8–3.6 J/mm^2. One week after intravitreal injection and NOD, the mice were sacrificed, and the retinal cup was extracted and imaged using confocal fluorescence microscopy. For a 1-h incubation of fGNRs, Figure 5J shows representative fluorescence images of the retina transfected at 1.8 J/mm^2 and of the control (no fGNRs or plasmid). Quantification of expression (measured by fluorescence intensity) in retina for two different NOD laser doses (Figure 5J) shows optimal transfection at 1.8 J/mm^2. For overnight incubation of fGNRs, the optimal dose was found to be 3.6 J/mm^2 (Figure 5K). The inset images in Figure 5K show representative fluorescence images of the retina transfected using a 3.6 J/mm^2 laser dose and no fGNRs/plasmids (control). The significant difference in fluorescence intensity of retina between the NOD eye and control shows delivery of MCO-II-mCherry plasmids into targeted retina using a CW NIR laser beam.

To determine the type of cells that are transfected by NOD after intravitreal injection of CAG-MCO-II-mCherry plasmids, we carried out

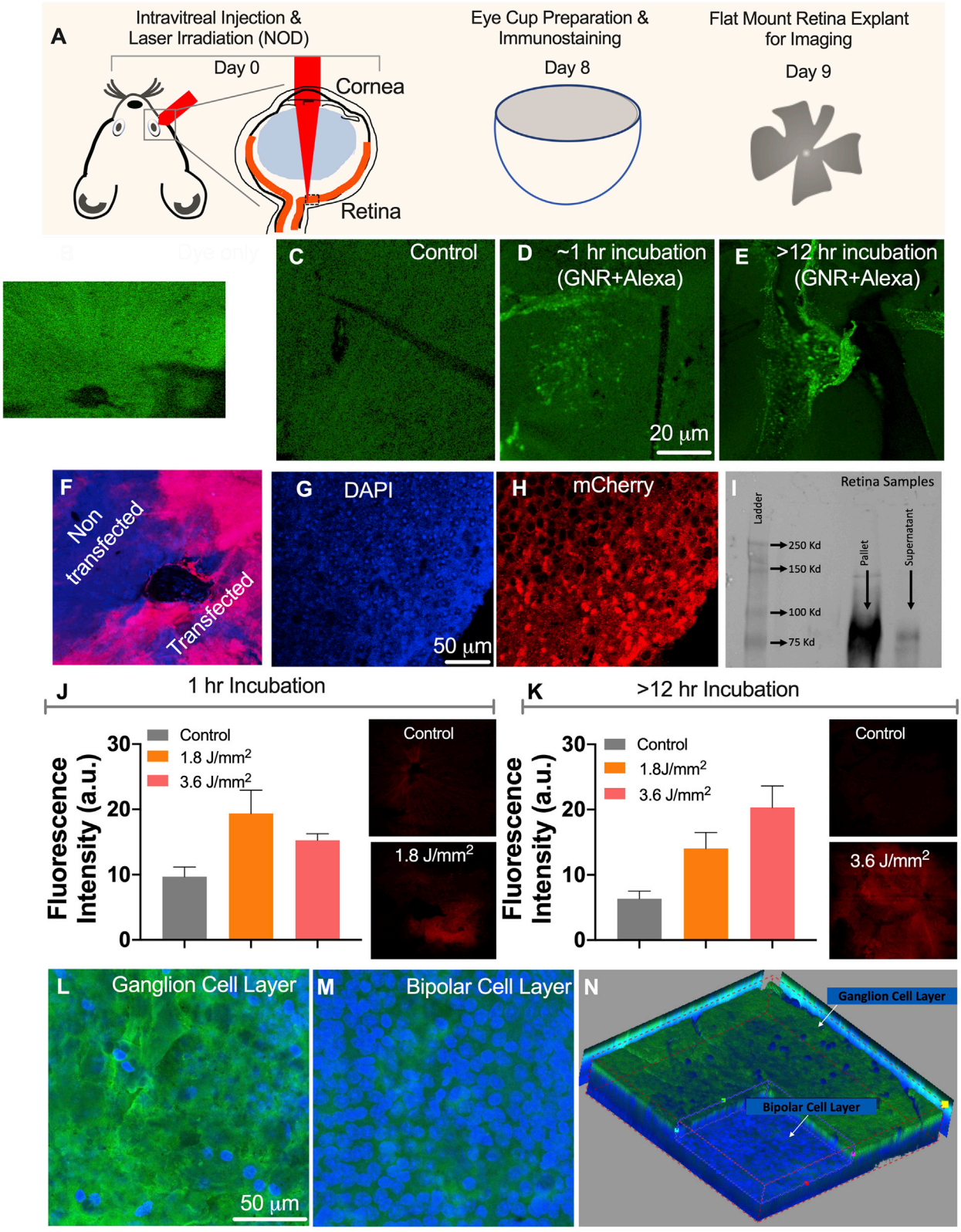

(legend on next page)

cell-specific immunostaining of the NOD-transected retina of *rd10* mice. Fluorescence images of retina, after *in vivo* optical delivery using a CW 1,064-nm laser beam, stained with the nuclear stain DAPI (Figure S6A) and the retinal ganglion cell (RGC)-specific stain POU4F1 (Figure S6B), are overlaid on a fluorescence image of reporter-mCherry expressed in retina (Figure S6C). The composite image shows co-localization of RGCs with mCherry expression. The high degree of co-localization suggests that *in vivo* NOD of retina, after intravitreal injection, is RGC specific. This is due to the fact that both fGNRs and plasmids were injected intravitreally, which leads to significant binding with the proximal RGC layer. Furthermore, confocal fluorescence images of immunostained retina (after NOD) show the presence of MCO-reporter (mCherry) in the RGC layer (Figure 5L), and not in the bipolar cell layer (Figure 5M). Three-dimensional reconstruction of retina (Figure 5N) shows RGC layer-specific expression of MCOs achieved by *in vivo* NOD.

Evaluation of Macrophages in Retina Due to Injection of fGNRs and Subsequent Laser Irradiation

Immunostaining of the retinal section was carried out in order to evaluate the induction of macrophages due to fGNR (GNRs functionalized with Con A)-mediated NOD. Figure 6 represents confocal images of immunostained retinal sections. The expression of mCherry in ganglion cells is evident by distinct red fluorescence (secondary antibody fluorescence, Alexa Fluor 594). In order to assess macrophage induction due to NOD and fGNRs, the retina samples were co-stained for macrophage markers (CD68) and imaged in the green channel (DyLight 488). No detectable macrophage induction was observed in the immunostained retina samples (Figure 6A) when compared to the control eye (Figure 6B: absence of fGNRs and NOD), suggesting that the presence of Con A-conjugated GNRs and laser irradiation did not cause a macrophage-related immunoresponse in the eye.

Visually Evoked Spiking Activities Confirmed Communication between the NOD-Enabled, MCO-II-Sensitized Retina and Visual Cortex

In order to evaluate the functional recovery of degenerated retina and establishment of communication with the visual cortex, visually evoked spiking activities were monitored in the visual cortex of *rd10* mice, having NOD-enabled, MCO-II sensitized RGCs. The *rd10* mice have a later onset and progressive retinal degeneration, closer to the human retinal degeneration phenotype. At the age of 12 weeks, complete loss of photoreceptors was observed in *rd10* mice as measured by spectral domain optical coherence tomography (SDOCT) imaging (before laser delivery) and immunostaining with visual arrestin after sacrificing the mice. For visual stimulation of the NOD or other control eye, white light-emitting diode (LED)-emitting broad spectral light (400–650 nm) was pulsated at 1 Hz (200 ms ON, 800 ms OFF). A 16-channel multi-electrode array (MEA) and acquisition system (Plexon) was used to map the visual cortex 1 (V1) activities (Figure 7A). Visual cortex activities in mice having one eye sensitized with MCO-II by NOD (CW 1,064 nm) subsequent to light stimulation using different intensities (1, 10, 80, and 220 cd·s/m^2) were measured in V1 (Figure 7B, top panel). In the bottom panel of Figure 7B, we show spiking activities in the visual cortex (V1) at the same electrode location of the animal subsequent to visual stimulation of the PBS-injected eye using no light, and light with different intensities. Figure 7C quantitatively compares the visually evoked spiking activities in V1 of *rd10* mice in response to light stimulation in the NOD-enabled, MCO-II sensitized eye and in the PBS-injected eye. Unlike the PBS-injected eye, the V1-spiking activities increased with increases in the light intensities. The mice were sacrificed after measurement of visually evoked spiking activities and retinas were immunostained for mCherry expression analysis. In Figure 7D, we show a confocal fluorescence image of an immunostained retina having expression of MCO-II-mCherry.

In Vivo NOD of MCO-II to *rd10* Mice Does Not Compromise Viability of Retina or Elicit an Immune Response

To evaluate safety of *in vivo* NOD-based gene delivery, we conducted an apoptosis assay on mouse retina to assess the viability of retina using a caspase marker. Figure S7A shows fluorescence images of retina stained with caspase-3 (green) and DAPI (blue) for two different CW laser doses (dose 1, 1.8 J/mm^2; dose 2, 3.6 J/mm^2). The apoptotic cells were not detected after optical delivery using a CW laser beam. Next, in order to determine the immune response subsequent to NOD, we carried out CD45 immunostaining of the CW laser-irradiated retina (Figure S7B). No detectable CD45 (red) signal suggests the absence of immune cells after MCO-II transfection by the laser at doses of 0.9 and 1.8 J/mm^2. These results demonstrate that *in vivo* optical delivery of MCO-II to *rd10* mouse retina does not compromise viability of retina or elicit an immune response.

DISCUSSION

The results clearly demonstrate that the proposed NOD method is a viable, minimally invasive approach to remotely guide delivery of

Figure 5. *In Vivo* Spatially Targeted, Layer-Specific Delivery of MCO-II into Retina by CW Near-Infrared Laser Beam-Based NOD Using fGNRs with an SPR Peak-Matching NOD Laser Beam

(A) Schematic representation of *in vivo* NOD in *rd10* mouse eye and subsequent steps to visualize the expression. (B and C) Fluorescence image of retina: (B) after intravitreal injection of fluorescence (Alexa Fluor 488) dye and (C) control (no dye injection). (D and E) Confocal fluorescence image of retina after intravitreal injection of fluorescence dye-labeled functionalized gold nanorods (fGNRs) with the surface plasmon resonance (SPR) peak at 1,064 nm: (D) ~1 h after injection and (E) overnight (>12 h) incubation. (F) Immunostained confocal image of NOD-treated mice retina, showing the expression of MCO-II-mCherry (red) overlaid on nuclear stain DAPI (in blue). (G and H) Higher magnification image of retinal cells: (G) DAPI and (H) mCherry. The laser dose was 600 mJ/mm^2 (20 mW for 30 s, 1-mm^2 area). (I) Chemiluminescent western blot of retinal cell extract after *in vivo* transfection of MCO-II-mCherry by NOD. The immunoprecipitated retinal lysate shows distinct mCherry. (J and K) Quantification of expression (measured by fluorescence intensity) in retina for different NOD laser doses: (J) with 1-h incubation of fGNRs and (K) overnight incubation of fGNRs. Mean + SD. Insets: representative fluorescence images of retina for control and NOD-transfected retinas. (L and M) Confocal fluorescence images of immunostained MCO-reporter (mCherry) in (L) RGC and (M) bipolar cell layers. (N) RGC layer-specific expression of MCO achieved by *in vivo* NOD (3D-stacked confocal image of retina).

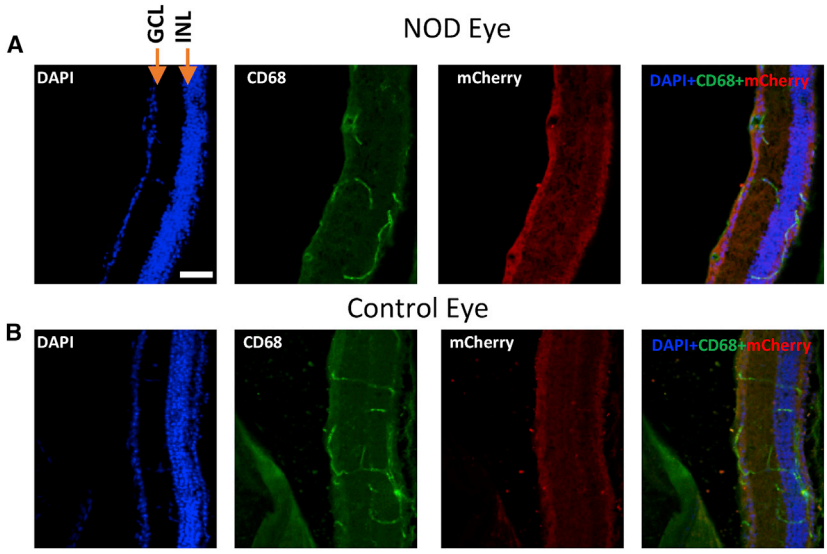

Figure 6. Evaluation of Presence of Macrophages in the Targeted NOD Area of Retina

(A) Immunostained images of transfected retinal section of spatially targeted NOD area for evaluation of the presence of macrophages (green) and the presence of mCherry expression in the ganglion cell layer (red). DAPI and composite images are also presented. (B) Identical immunostained images of a control section of retina from the contralateral eye are presented for comparison. The mCherry expression was observed in the ganglion cell layer in the NOD eye retinal section. No significant presence of microphage was detected in the NOD eye retina. Scale bar, ~50 μm. GCL, ganglion cell layer; INL, inner nuclear layer.

therapeutic genes to targeted cells *in vitro* as well as *in vivo*. Since the gold nano-structures have very low cytotoxicity[41] and have been widely used in various clinical trials (ClinicalTrials.gov: NCT03020017, NCT02837094, and NCT01270139) they present an ideal nanomaterial for clinical translation of the NOD method. The nanoparticles travel to retina via diffusion from the vitreous. To allow such diffusion, a 1- to 12-h incubation time is provided after nanoparticle injection for NOD to occur. Over time, the nanoparticles injected in the vitreous are known to get cleared from the vitreous.[41] Compared with pulsed lasers, CW NIR (diode) lasers are compact, easy to use, and therefore have significant translational potential. For example, targeted *in vivo* optical delivery of opsin genes to degenerated retinal regions in dry-AMD patients using a NIR laser beam in a safe manner will enable restoration of photosensitivity in the geographic atrophy areas. In progressive retinal degenerative diseases such as dry-AMD, degeneration of retina advances at ~2 mm^2 per year and varies from person to person. During such progressive loss, NOD can be easily repeated, allowing gene (e.g., MCO) expression in newly degenerated retinal areas.

In the NOD method, the contrast in temperature rise in laser-irradiated nanorod-attached cells at nano-hotspots is significant enough to allow site-specific delivery of large plasmids (e.g., MCO-II-mCherry). Unlike focused ultrafast laser-based optoporation,[37] the NOD technology is easy to adapt in the clinical setting since it puts no restriction on maintaining the focal plane with a target layer. Furthermore, it provides increased sensitivity of targeted cells with no detectable collateral damage. By varying the shapes of functionalized field-enhancing GNRs[42–50] that bind to targeted cell types, tuning the NIR laser wavelength will allow wavelength-selective enhancement near specific cells and thus selective delivery. In the NOD method, the presence of GNRs (fGNRs) is required only during the laser irradiation for gene delivery. As demonstrated in this study, the NOD procedure is completed within 1–12 h of injection. Once the genes are delivered onto the targeted cells and tissue, the presence of fGNRs is not required, and gene expression occurs via protein translation. The NOD-based transfection is highly specific to targeted cells. The spatially targeted expression is achieved and controlled by the presence of three key components at the same spatial location: (1) fGNRs, (2) targeted laser irradiation, and (3) plasmids containing specific promoters. The non-targeted areas (absence of laser irradiation) will not have transfection even though the plasmids and fGNRs are present.

For use of NOD in eyes of human subjects, the NIR laser beam for NOD may be integrated with ophthalmic viewing devices such as a slit lamp or OCT for obtaining feedback. After identifying the pathological areas that need treatment, the subject's eye(s) can be injected with fGNRs and therapeutic molecules into the vitreous cavity or sub-retinal space depending on the targeted retinal layer, followed by NIR laser beam irradiation targeted to the pathological region(s) of interest. In case of rapid movement of the organ (e.g., eye), it may be advantageous to use a spatially sculpted NIR beam to match the shape of the region(s) of interest in the tissue requiring targeted molecular delivery by NOD. In addition to motion artifacts, challenges in perfectly matching the margins of the NIR laser for NOD may arise due to scattering tissue and imperfect optical media of the eye. To correct for wave-front distortions in the NOD laser beam, implementation of adaptive optics may be required for improving the performance of the NOD process. This is accomplished by compensating for the higher order aberrations originating from the cornea and the lens of the eye by using a deformable adaptive optics mirror. While continuous exposure to an NIR laser beam can be used to accomplish such NOD, the laser may be pulsed (width varying from several microseconds to seconds) in order to optimize delivery without overall heating of the cells/tissues.

Although the present study demonstrates spatially targeted delivery of MCO to the retina by use of a laser beam, this technique will be applicable for delivery of other large therapeutic genes such as ABCA4 for Stargardt's disease,[51] USH genes for Usher's syndrome,[52] and CEP290 for Leber congenital amaurosis,[53] as well as large CRISPR constructs for correcting gene mutations.[54] NOD-based gene expression lasts for several weeks, and such short-term expression may be

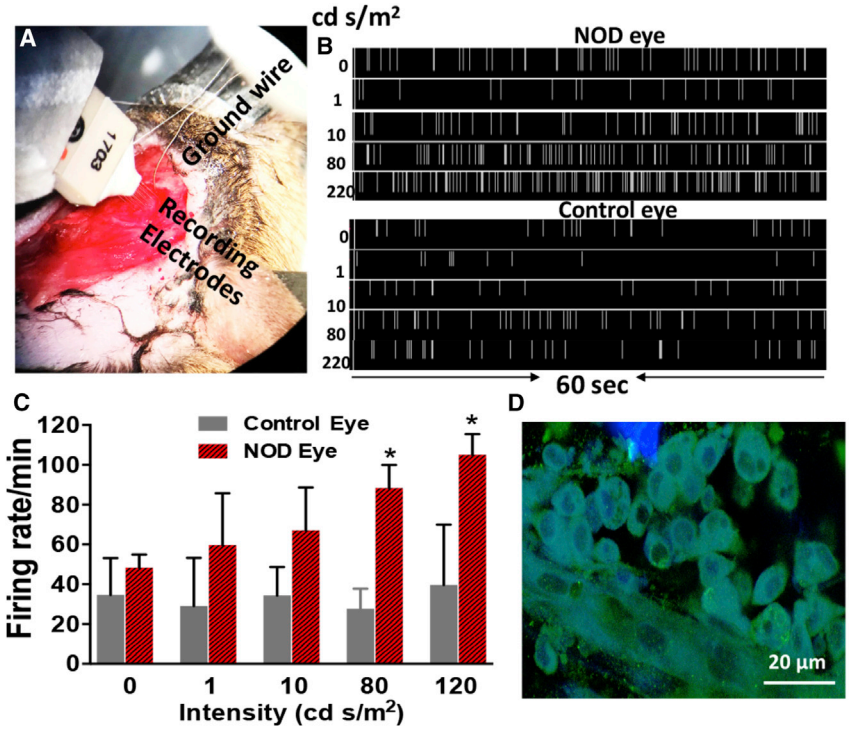

Figure 7. Visually Evoked Spiking Activities Observed in Visual Cortex of *rd10* Mice Having NOD-Enabled, MCO-II-Sensitized RGCs

(A) Setup for measuring visually evoked spiking activities in V1. (B) Top: spiking activities in visual cortex (V1) subsequent to visual stimulation of the MCO-II-expressing eye using no light and light with intensities of 1, 10, 79, and 220 cd·s/m^2. Bottom: spiking activities in visual cortex (V1) at the same electrode location of the animal subsequent to visual stimulation of the PBS-injected eye using no light and light with intensities of 1, 10, 80, and 220 cd·s/m^2. The visual stimulation light pulses were applied at 1 Hz (200 ms ON, 800 ms OFF) for 60 s. (C) Visual stimulation intensity-dependent cortical activities in *rd10* mice. Mean + SD. *p < 0.05 between control and NOD eye. (D) Confocal fluorescence image of immunostained retina, showing the expression of MCO-II-mCherry in RGCs.

advantageous for several aspects, including (1) in some cases such as chimeric antigen receptor (CAR)-T cancer therapy[55] and acute lung injuries by providing a clinically meaningful outcome, and (2) it allows evaluation of an acute therapeutic response (if any) before exposing the subjects or population to a chronic irreversible genetic change such as CRISPR.[54] For long-term expression, novel capsid-free, close-ended[56] linear duplex genes comprised of an inverted terminal repeat (ITR) can be delivered by the NOD method described herein.

Conclusions

The *in vitro and in vivo* results clearly demonstrated that large (MCO-II-mCherry) plasmids can be introduced into cells in a minimally invasive manner by nano-enhanced effects using a CW and nanosecond-pulsed NIR laser beam (1,064 nm). Furthermore, our results clearly demonstrate gene delivery and functional cellular expression in targeted regions of retina using a CW NIR laser beam without compromising the cell viability. Our results show an increase in visually evoked spiking activities, in mice with NOD-transfected, MCO-II-sensitized retina, confirming communication between functionalized retina and the visual cortex. Safe NOD-mediated molecular delivery has the potential for effective gene therapy of diverse retinal degenerations in patients.

MATERIALS AND METHODS

Ethics Statement

All experimental procedures were conducted according to the Nanoscope Technologies Institutional Animal Care and Use Committee (IACUC)-approved protocol.

MCO-II Plasmid

A high-throughput DNA synthesizer was used to synthesize the parent DNA fragment coding for MCO-II with the restriction enzymes BamHI and SalI. The gene was built using a plasmid adeno-associated virus (pAAV) vector with a CAG promotor, trafficking signal sequence, and fluorescent reporter protein (mCherry). Purified plasmid DNA of MCO-II-mCherry was prepared for NOD. The sequence of the DNA construct was confirmed with sequence analysis.

Intravitreal Injection of MCO-II to the *rd10* and Wild Type Mouse Eye

An aseptic technique was used for all surgical procedures, and surgical tools were sterilized by autoclaving. The mouse was anesthetized and local anesthesia (proparacaine) was instilled into the eye of the animal. The MCO-II (1 µL) solution was injected by a sterilized 29G needle of a Hamilton microsyringe inserted through the sclera into the vitreous cavity (intravitreal injection). For controls, 1 µL of PBS was injected into the eye intravitreally by a sterilized 29-gauge needle. The cornea was kept moist with a balanced salt solution during the surgical procedure.

GNRs and Functionalization

Con A-conjugated GNRs (aspect ratio, 6.7) with the SPR maximum at 1,064 nm was used for NOD experiments. The GNRs were treated with Con A molecules (4 µM) to facilitate the binding of a GNR with membrane of the targeted cells. 1 mL of GNR solution (0.035 mg/mL) was centrifuged at 13,000 rpm for 15 min and resuspended in Con A solution, then incubated at 37°C for 12 h. The mixture of Con A and the GNR complex was re-dispersed in 10 mM HEPES (*N*-2-hydroxyethylpiperazine-*N*′-2-ethanesulfonic acid) buffer (pH 7.4) after 12 h of incubation. Prior to resuspension in the HEPES buffer, the unbound Con A molecules were removed by centrifugation at room temperature.

Cell Culture and Transfection

HEK293 cells were cultured in a sterile Petri dish (35 mm) and maintained in DMEM/F-12 cell culture media, supplemented with 10% fetal bovine serum (FBS) (Sigma-Aldrich), streptomycin (0.2 mg/mL, Sigma-Aldrich), and penicillin (200 U/mL Sigma-Aldrich). The cultures were maintained at 37°C in a 5% CO_2 humidified atmosphere. 48 h after plating, the cells were incubated with GNRs (1,064 nm). After a further 2 h, the MCO-II plasmids were added into the cell culture medium and incubated for 15 min. The cells were then exposed with a nanosecond (1,064 nm) or CW (1,064 nm) laser beam with different intensities and exposure times. The cells were then moved back to 37°C in a 5% CO_2 humidified atmosphere.

Western Blot Assay

Western blot experiments were performed to confirm expression of the MCO-II-mCherry protein by using an anti-mCherry antibody (NBP1-96752, Novus Biologicals). Briefly, cultured HEK293 cells were transfected with MCO-II-mCherry by NOD or jetPRIME (positive control). After 3 days of transfection, the cells were collected and then pelleted by centrifugation. The pellet was lysed in RIPA buffer (10 mM Tris-Cl [pH 8.0], 2 mM EDTA, 1% Triton X-100, 0.5% sodium deoxycholate, 0.1% SDS, and 150 mM NaCl) in the presence of protease inhibitor cocktail (Thermo Scientific, #78440). For *in vivo* NOD, retinal cells in wild-type mice (N = 5) were transfected with MCO-II-mCherry plasmids. After 1 week of transfection, the retina was freshly harvested and lysed in RIPA buffer as done *in vitro* for cells. A clear supernatant for *in vitro* as well as *in vivo* NOD samples containing the protein was collected after centrifugation at 14,000 × *g* for 5 min. The total protein concentration was measured by a Pierce 660-nm protein assay (Thermo Fisher Scientific). The supernatant was transferred to an Eppendorf tube and immunoprecipitation was performed using mouse anti-mCherry protein. The antibody/antigen complex was then pulled out using protein G-agarose beads (Pierce). Immunoprecipitated MCO-II-mCherry protein was separated by 4%–15% pre-made gradient gels (Bio-Rad), and proteins were transferred for 1 h at 120 V onto nitrocellulose membranes. Membranes were blocked in skim milk for 60 min followed by incubation with anti-mCherry (overnight at 4°C). Membranes were washed twice (5 min each) and then incubated with the secondary antibody horseradish peroxidase-conjugated anti-mouse immunoglobulin G (IgG) for 30 min (1:10,000; GE Healthcare, Piscataway, NJ, USA). Chemiluminescence was developed using a SuperSignal West Dura kit (Thermo Scientific) and the blot was imaged.

Mice Model with Retina Degeneration

Approximately 12-week-old retinal degenerated mice (B6.CXB1-*Pde6b*^{rd10}/J, Jackson Laboratory) and wild type mice (C57BL/6J, Jackson Laboratory) were used in the reported *ex vivo* and *in vivo* experiments. All aspects of experimental procedures on the animals were in strict accordance with guidelines of the Nanoscope Technologies IACUC. Mice were maintained on a 12-h light/12-h dark cycle.

Retinal Explant: *Ex Vivo* Transfection

Adult *rd10* mice were sacrificed using CO_2 inhalation. The eyes of *rd10* mice were surgically removed from their muscles and remaining orbital contents and then choroid, sclera, cornea, lens, and vitreous were then removed from the enucleated eye. The retina was incubated with fresh Neurobasal medium. The retinal pigment epithelium (RPE) was gently removed from the retina, and retina explants were cut into pieces using a tissue chopper. The explants were placed onto sterilized Petri dishes previously coated with 5 μg of poly-D-lysine per dish containing 1 mL of Neurobasal medium. The explants were incubated with Con A-conjugated GNRs for 2 h at 37°C in a humidified 5% CO_2 incubator. The CAG-MCO-II-mCherry plasmid was added directly onto the retina explants for 15 min, and NOD was carried out using a 1,064-nm CW or pulsed laser beam.

In Vivo NOD Experiments: Mouse Preparation and Transduction of MCO-II mCherry

Prior to the *in vivo* experiments, the mice were anesthetized using the mixture of 90 mg/kg ketamine, 10 mg/kg xylazine, and 0.5 mg/kg acepromazine. Tropicamide (1%) was used to dilute the pupils of the mice. Sterile proparacaine hydrochloride ophthalmic solution (0.5%) eye drops were administered to provide topical anesthesia. A dissection microscope and sterilized 32G needle of a Hamilton micro-syringe were used to perform the intravitreal injection of MCO-II mCherry plasmids and fGNRs (SPR at 1,064 nm). Ciprofloxacin (0.3%) eye drops were applied to the ocular surface following the intravitreal injection. The cornea was kept moist with a balanced salt solution during the entire surgical procedure. Reversal of anesthetic was achieved by intraperitoneal injection of normal sterile 0.9% saline solution (400 μL). After 1 week of transfection, the animals were euthanized, and retinal tissues were explanted for immunostaining or western blot.

Immunostaining

The NOD-treated and non-treated samples (HEK cells, retinal explants, and mouse eyes) were fixed in modified Davidson solution overnight and finally stored in 1× PBS. Next, the eyecup and retinal section were prepared and subjected to 0.5% Triton X-100 (washing solution) three times. The nonspecific binding of antibodies was blocked by 4% serum for 60 min, after which they were washed with washing solution three times. The samples were incubated with primary antibodies (1:500 dilution), e.g., anti-mCherry, POU4F1, caspase-3, CD45, and CD68, overnight at 4°C. After washing samples with 0.5% Triton X-100 solution in 1× PBS three times, secondary antibody (goat anti-rabbit Alexa Fluor 488 or goat anti-mouse Alexa Fluor 594), diluted 1:250 in washing solution, was loaded for 1 h at room temperature. The samples were then stained with DAPI (1 μg/ml).

Confocal Fluorescence Imaging

The NOD-treated *ex vivo* (HEK cells and retinal explants) and *in vivo* (explanted retinal tissues) samples were immunostained to identify and quantify the mCherry expression. Prior to imaging, the samples were washed with 1× PBS. Images were taken by a confocal

microscope (Olympus Fluoview FV1000) using the laser with excitation lines at 405 nm (DAPI), 488 nm (Alexa Fluor 488), and 543 nm (Alexa Fluor 594). Image processing was performed using ImageJ software.

Statistical Analysis

GraphPad Prism was used to analyze data. The data were plotted as mean ± SD. Statistically significant difference analyses were carried out by a t test. $p < 0.05$ was considered statistically significant.

SUPPLEMENTAL INFORMATION

Supplemental Information can be found online at https://doi.org/10.1016/j.omtm.2020.03.030.

AUTHOR CONTRIBUTIONS

S.B., S.G., and S.M. carried out the NOD and confocal microscopy experiments. S.G. prepared the plasmids and fGNRs. S.B. and S.G. performed immunohistochemistry and carried out the data analysis. S.B. and S.M. performed the visually evoked activity measurements. S.M. and A.D. performed intravitreal injections. A.D. and K.T. helped in performing western blots. W.W. provided input and participated in discussions. S.M. designed the experiments and supervised the project. The manuscript was written through contributions of all authors.

CONFLICTS OF INTEREST

S.M. has an equity interest in Nanoscope Technologies LLC. The remaining authors declare no competing interests.

ACKNOWLEDGMENTS

This work was supported in part by the National Institutes of Health (1R43EY026483-01, 1R43EY025905-01, 1R01EY025717-01A1, 1R01EY028216-01A1, and 2R44EY025905-02A1). The authors would also like to thank Melissa Galicia for animal care.

REFERENCES

1. Somia, N., and Verma, I.M. (2000). Gene therapy: trials and tribulations. Nat. Rev. Genet. *1*, 91–99.
2. Verma, I.M., and Somia, N. (1997). Gene therapy—promises, problems and prospects. Nature *389*, 239–242.
3. Luo, D., and Saltzman, W.M. (2000). Synthetic DNA delivery systems. Nat. Biotechnol. *18*, 33–37.
4. Mohanty, S.K., Reinscheid, R.K., Liu, X., Okamura, N., Krasieva, T.B., and Berns, M.W. (2008). In-depth activation of channelrhodopsin 2-sensitized excitable cells with high spatial resolution using two-photon excitation with a near-infrared laser microbeam. Biophys. J. *95*, 3916–3926.
5. (2011). Method of the year 2010. Nat. Methods *8*, 1.
6. Deisseroth, K. (2011). Optogenetics. Nat. Methods *8*, 26–29.
7. Fenno, L., Yizhar, O., and Deisseroth, K. (2011). The development and application of optogenetics. Annu. Rev. Neurosci. *34*, 389–412.
8. Pastrana, E. (2011). Optogenetics: controlling cell function with light. Nat. Methods *8*, 24–25.
9. Shivalingaiah, S., Gu, L., and Mohanty, S.K. (2011). Non-linear stimulation of excitable cells with and without optogenetic sensitization. Proc. SPIE *7883*, 788355.
10. Nagel, G., Szellas, T., Huhn, W., Kateriya, S., Adeishvili, N., Berthold, P., Ollig, D., Hegemann, P., and Bamberg, E. (2003). Channelrhodopsin-2, a directly light-gated cation-selective membrane channel. Proc. Natl. Acad. Sci. USA *100*, 13940–13945.
11. Boyden, E.S., Zhang, F., Bamberg, E., Nagel, G., and Deisseroth, K. (2005). Millisecond-timescale, genetically targeted optical control of neural activity. Nat. Neurosci. *8*, 1263–1268.
12. Aravanis, A.M., Wang, L.P., Zhang, F., Meltzer, L.A., Mogri, M.Z., Schneider, M.B., and Deisseroth, K. (2007). An optical neural interface: in vivo control of rodent motor cortex with integrated fiberoptic and optogenetic technology. J. Neural Eng. *4*, S143–S156.
13. Zhang, F., Aravanis, A.M., Adamantidis, A., de Lecea, L., and Deisseroth, K. (2007). Circuit-breakers: optical technologies for probing neural signals and systems. Nat. Rev. Neurosci. *8*, 577–581.
14. Johansen, J.P., Hamanaka, H., Monfils, M.H., Behnia, R., Deisseroth, K., Blair, H.T., and LeDoux, J.E. (2010). Optical activation of lateral amygdala pyramidal cells instructs associative fear learning. Proc. Natl. Acad. Sci. USA *107*, 12692–12697.
15. Tønnesen, J., Parish, C.L., Sørensen, A.T., Andersson, A., Lundberg, C., Deisseroth, K., Arenas, E., Lindvall, O., and Kokaia, M. (2011). Functional integration of grafted neural stem cell-derived dopaminergic neurons monitored by optogenetics in an *in vitro* Parkinson model. PLoS ONE *6*, e17560.
16. Adamantidis, A.R., Tsai, H.C., Boutrel, B., Zhang, F., Stuber, G.D., Budygin, E.A., Touriño, C., Bonci, A., Deisseroth, K., and de Lecea, L. (2011). Optogenetic interrogation of dopaminergic modulation of the multiple phases of reward-seeking behavior. J. Neurosci. *31*, 10829–10835.
17. Alilain, W.J., Li, X., Horn, K.P., Dhingra, R., Dick, T.E., Herlitze, S., and Silver, J. (2008). Light-induced rescue of breathing after spinal cord injury. J. Neurosci. *28*, 11862–11870.
18. Ivanova, E., Roberts, R., Bissig, D., Pan, Z.-H., and Berkowitz, B.A. (2010). Retinal channelrhodopsin-2-mediated activity in vivo evaluated with manganese-enhanced magnetic resonance imaging. Mol. Vis. *16*, 1059–1067.
19. Lagali, P.S., Balya, D., Awatramani, G.B., Münch, T.A., Kim, D.S., Busskamp, V., Cepko, C.L., and Roska, B. (2008). Light-activated channels targeted to ON bipolar cells restore visual function in retinal degeneration. Nat. Neurosci. *11*, 667–675.
20. Shivalingaiah, S., Gu, L., and Mohanty, S.K. (2011). Correlation of spatial intensity distribution of light reaching the retina and restoration of vision by optogenetic stimulation. Proc. SPIE *7885*, 78851Y.
21. Zufferey, R., Nagy, D., Mandel, R.J., Naldini, L., and Trono, D. (1997). Multiply attenuated lentiviral vector achieves efficient gene delivery in vivo. Nat. Biotechnol. *15*, 871–875.
22. Ruitenberg, M.J., Eggers, R., Boer, G.J., and Verhaagen, J. (2002). Adeno-associated viral vectors as agents for gene delivery: application in disorders and trauma of the central nervous system. Methods *28*, 182–194.
23. Naldini, L., Blömer, U., Gallay, P., Ory, D., Mulligan, R., Gage, F.H., Verma, I.M., and Trono, D. (1996). In vivo gene delivery and stable transduction of nondividing cells by a lentiviral vector. Science *272*, 263–267.
24. Thomas, C.E., Ehrhardt, A., and Kay, M.A. (2003). Progress and problems with the use of viral vectors for gene therapy. Nat. Rev. Genet. *4*, 346–358.
25. King, R. (2004). Gene delivery to mammalian cells by microinjection. Methods Mol. Biol. *245*, 167–174.
26. Li, S., and Huang, L. (2000). Nonviral gene therapy: promises and challenges. Gene Ther. *7*, 31–34.
27. Ferber, D. (2001). Gene therapy. Safer and virus-free? Science *294*, 1638–1642.
28. Newman, C.M., Lawrie, A., Brisken, A.F., and Cumberland, D.C. (2001). Ultrasound gene therapy: on the road from concept to reality. Echocardiography *18*, 339–347.
29. Templeton, N.S., Lasic, D.D., Frederik, P.M., Strey, H.H., Roberts, D.D., and Pavlakis, G.N. (1997). Improved DNA: liposome complexes for increased systemic delivery and gene expression. Nat. Biotechnol. *15*, 647–652.
30. Panyam, J., and Labhasetwar, V. (2003). Biodegradable nanoparticles for drug and gene delivery to cells and tissue. Adv. Drug Deliv. Rev. *55*, 329–347.
31. Schubert, R., Trenholm, S., Balint, K., Kosche, G., Cowan, C.S., Mohr, M.A., Munz, M., Martinez-Martin, D., Fläschner, G., Newton, R., et al. (2018). Virus stamping for targeted single-cell infection in vitro and in vivo. Nat. Biotechnol. *36*, 81–88.
32. Grunwald, J.E., Pistilli, M., Ying, G.S., Maguire, M.G., Daniel, E., and Martin, D.F.; Comparison of Age-related Macular Degeneration Treatments Trials Research

Group (2015). Growth of geographic atrophy in the comparison of age-related macular degeneration treatments trials. Ophthalmology *122*, 809–816.

33. Wu, Z., Ayton, L.N., Luu, C.D., and Guymer, R.H. (2014). Microperimetry of nascent geographic atrophy in age-related macular degeneration. Invest. Ophthalmol. Vis. Sci. *56*, 115–121.

34. Wallsh, J., and Gallemore, R. (2015). Optical coherence tomography difference maps and average macular volume for geographic atrophy. Retin. Cases Brief Rep. *9*, 88–91.

35. Biarnés, M., Monés, J., Alonso, J., and Arias, L. (2011). Update on geographic atrophy in age-related macular degeneration. Optom. Vis. Sci. *88*, 881–889.

36. Sunness, J.S., Margalit, E., Srikumaran, D., Applegate, C.A., Tian, Y., Perry, D., Hawkins, B.S., and Bressler, N.M. (2007). The long-term natural history of geographic atrophy from age-related macular degeneration: enlargement of atrophy and implications for interventional clinical trials. Ophthalmology *114*, 271–277.

37. Dhakal, K., Batabyal, S., Wright, W., Kim, Y.-T., and Mohanty, S. (2015). Optical delivery of multiple opsin-encoding genes leads to targeted expression and white-light activation. Light Sci. Appl. *4*, e352.

38. Wright, W., Gajjeraman, S., Batabyal, S., Pradhan, S., Bhattacharya, S., Mahapatra, V., Tripathy, A., and Mohanty, S. (2017). Restoring vision in mice with retinal degeneration using multicharacteristic opsin. Neurophotonics *4*, 041505.

39. Mohanty, S.K., and Bhattacharya, S. (2017). Nano-enhanced optical delivery of exogenous molecules to cells and tissues. US patent WO/2017/139745, filed February 13, 2017, and granted August 17, 2017.

40. Batabyal, S., Gajjeraman, S., Bhattacharya, S., Wright, W., and Mohanty, S. (2020). Nano-enhanced optical gene delivery to retinal degenerated mice. Curr. Gene Ther. *19*, 318–329.

41. Masse, F., Ouellette, M., Lamoureux, G., and Boisselier, E. (2019). Gold nanoparticles in ophthalmology. Med. Res. Rev. *39*, 302–327.

42. Wang, S., Chen, K.J., Wu, T.H., Wang, H., Lin, W.Y., Ohashi, M., Chiou, P.Y., and Tseng, H.R. (2010). Photothermal effects of supramolecularly assembled gold nanoparticles for the targeted treatment of cancer cells. Angew. Chem. Int. Ed. Engl. *49*, 3777–3781.

43. Cheng, Y., Samia, A.C., Li, J., Kenney, M.E., Resnick, A., and Burda, C. (2010). Delivery and efficacy of a cancer drug as a function of the bond to the gold nanoparticle surface. Langmuir *26*, 2248–2255.

44. Kim, B., Han, G., Toley, B.J., Kim, C.K., Rotello, V.M., and Forbes, N.S. (2010). Tuning payload delivery in tumour cylindroids using gold nanoparticles. Nat. Nanotechnol. *5*, 465–472.

45. Tong, L., Zhao, Y., Huff, T.B., Hansen, M.N., Wei, A., and Cheng, J.X. (2007). Gold Nanorods mediate tumor cell death by compromising membrane integrity. Adv. Mater. *19*, 3136–3141.

46. Huang, X., El-Sayed, I.H., Qian, W., and El-Sayed, M.A. (2006). Cancer cell imaging and photothermal therapy in the near-infrared region by using gold nanorods. J. Am. Chem. Soc. *128*, 2115–2120.

47. Gobin, A.M., Lee, M.H., Halas, N.J., James, W.D., Drezek, R.A., and West, J.L. (2007). Near-infrared resonant nanoshells for combined optical imaging and photothermal cancer therapy. Nano Lett. *7*, 1929–1934.

48. Brongersma, M.L. (2003). Nanoshells: gifts in a gold wrapper. Nat. Mater. *2*, 296–297.

49. Chen, J., Wang, D., Xi, J., Au, L., Siekkinen, A., Warsen, A., Li, Z.-Y., Zhang, H., Xia, Y., and Li, X. (2007). Immuno gold nanocages with tailored optical properties for targeted photothermal destruction of cancer cells. Nano Lett. *7*, 1318–1322.

50. Chen, J., Saeki, F., Wiley, B.J., Cang, H., Cobb, M.J., Li, Z.-Y., Au, L., Zhang, H., Kimmey, M.B., Li, X., and Xia, Y. (2005). Gold nanocages: bioconjugation and their potential use as optical imaging contrast agents. Nano Lett. *5*, 473–477.

51. Molday, L.L., Rabin, A.R., and Molday, R.S. (2000). ABCR expression in foveal cone photoreceptors and its role in Stargardt macular dystrophy. Nat. Genet. *25*, 257–258.

52. Yan, D., and Liu, X.Z. (2010). Genetics and pathological mechanisms of Usher syndrome. J. Hum. Genet. *55*, 327–335.

53. Maeder, M.L., Stefanidakis, M., Wilson, C.J., Baral, R., Barrera, L.A., Bounoutas, G.S., Bumcrot, D., Chao, H., Ciulla, D.M., DaSilva, J.A., et al. (2019). Development of a gene-editing approach to restore vision loss in Leber congenital amaurosis type 10. Nat. Med. *25*, 229–233.

54. Scott, D.A., and Zhang, F. (2017). Implications of human genetic variation in CRISPR-based therapeutic genome editing. Nat. Med. *23*, 1095–1101.

55. June, C.H., O'Connor, R.S., Kawalekar, O.U., Ghassemi, S., and Milone, M.C. (2018). CAR T cell immunotherapy for human cancer. Science *359*, 1361–1365.

56. Zhang, Y., Liu, X., Zhang, J., and Zhang, C. (2016). Site-specific integration of CAR gene into Jurkat T cells with a linear close-ended AAV-based DNA vector for CAR-T engineering. Biotechnol. Lett. *38*, 1423–1431.

OMTM, Volume *17*

Supplemental Information

Near-Infrared Laser-Based Spatially Targeted Nano-enhanced Optical Delivery of Therapeutic Genes to Degenerated Retina

Subrata Batabyal, Sivakumar Gajjeraman, Kissaou Tchedre, Adnan Dibas, Weldon Wright, and Samarendra Mohanty

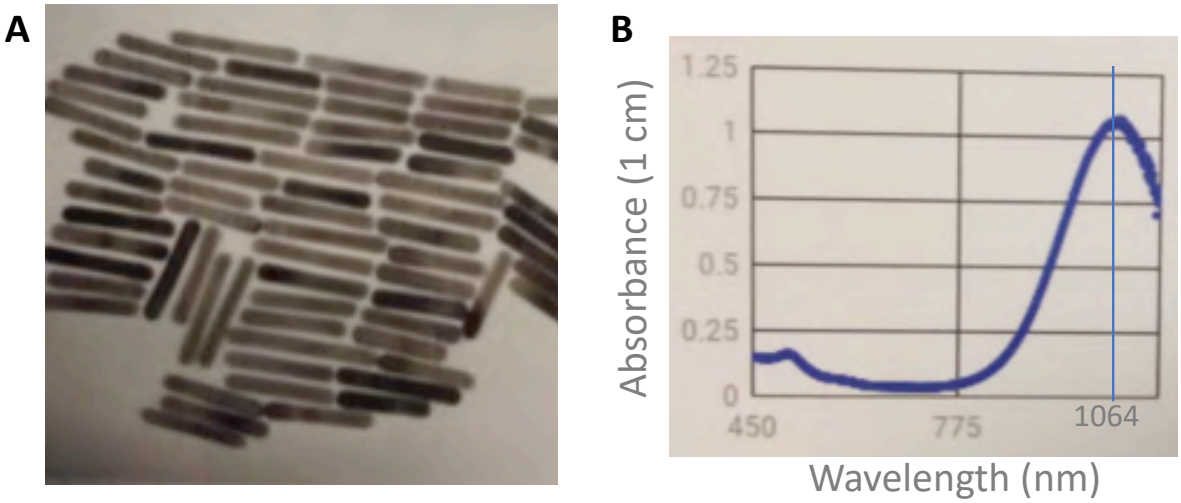

Suppl. Fig. 1. Structural and spectroscopic properties of gold nanorods. (A) Transmission electron microscopic image of gold nanorods used for nano enhanced optical delivery of CAG-MCO-II-mCherry into cells. These nanorods are functionalized with Concavalin A for binding of membrane of the cells. (B) Optical density of the gold nanorods, showing a peak at 1064 nm.

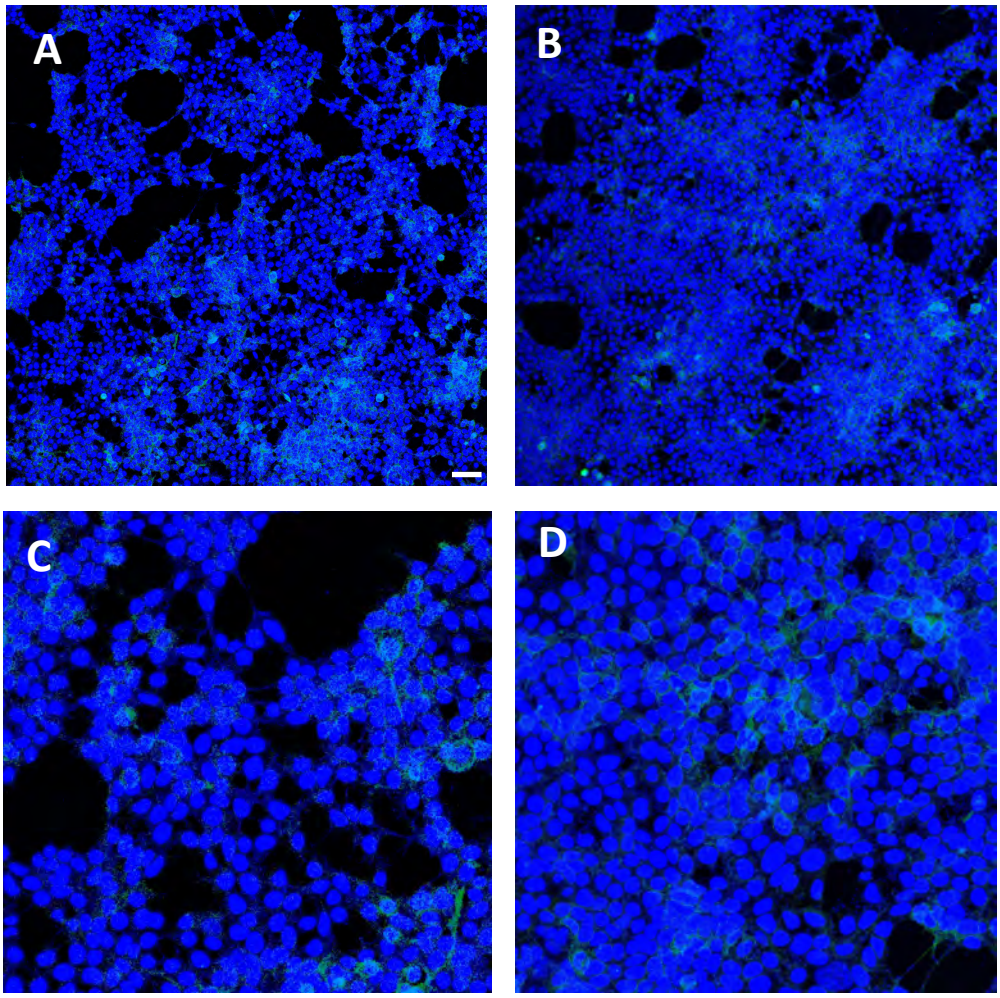

Suppl. Fig. 2. Confocal imaging of immunostained HEK cells for various experimental controls. (A) -Plasmid, - fGNR, - Laser; (B) + plasmids, + fGNRs - Laser. (C, D) 3x zoomed image of panels A and B, respectively. Primary antibody: Anti-mCherry, Secondary: Alexa 488. Nuclear stain: DAPI (blue). Scale bar = 50 μm.

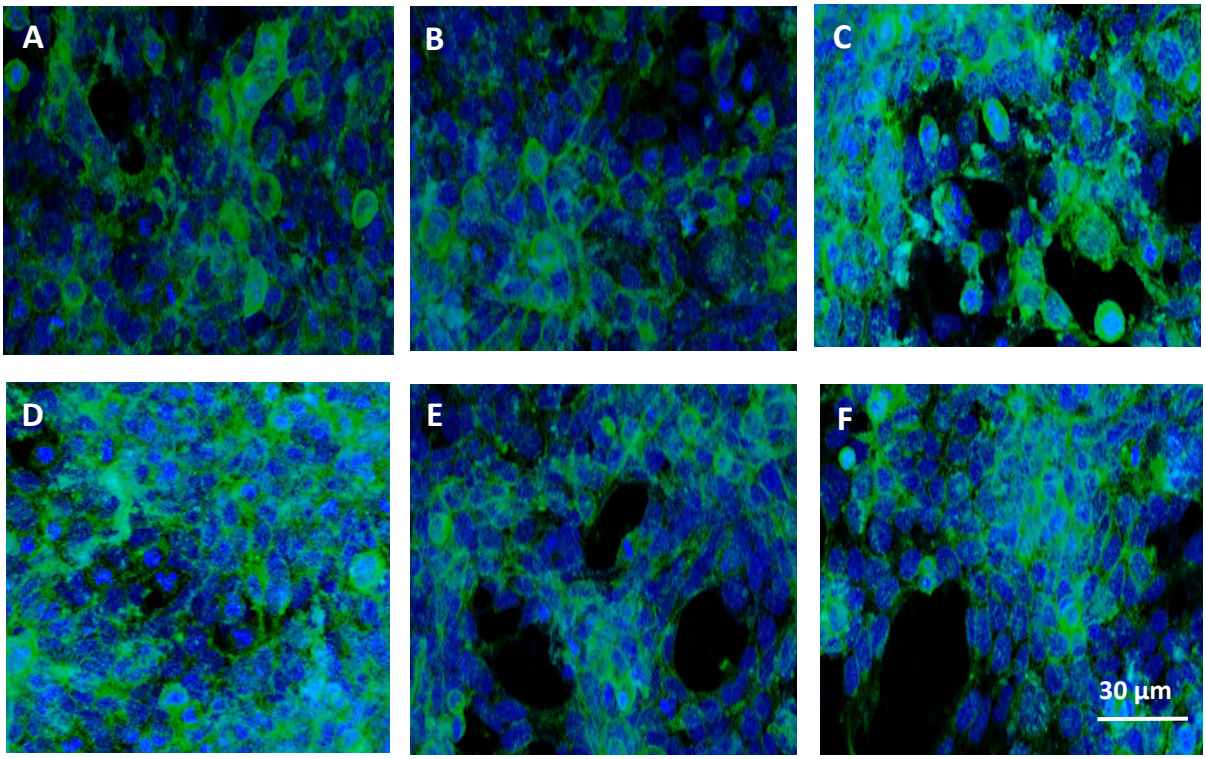

Suppl. Fig. 3. NOD treated HEK cells using 1064 nm Nanosecond laser beam with different pulse energy and exposure. (A) 2.5 mJ/mm^2 (10 mJ/pulse, 10 Hz, 5 s); (B) 5 mJ/mm^2 (20 mJ/pulse, 10 Hz, 5 s); (C) 7.5 mJ/mm^2 (30 mJ/pulse, 10 Hz, 5 s); (D) 5 mJ/mm^2 (10 mJ/pulse, 10 Hz, 10 s); (E) 10 mJ/mm^2 (20 mJ/pulse, 10 Hz, 10 s); and (F) 15 mJ/mm^2 (30 mJ/pulse, 10 Hz, 10 s). Energy density calculated using laser exposure area of 200 mm^2.

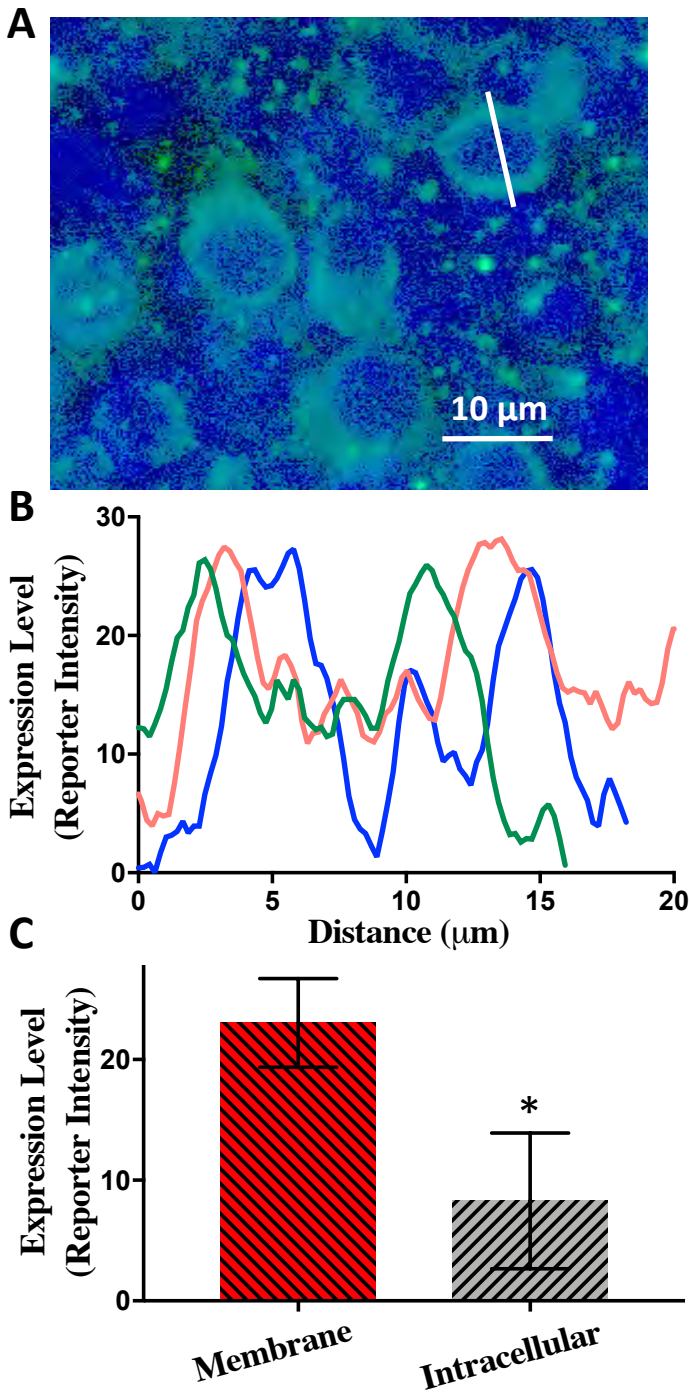

Suppl. Fig. 4. Cell specific expression in retina explant after nanosecond pulsed laser beam based NOD. (A) Retinal cells showing the expression of MCO-II-mCherry (Immunostained) after spatially targeted NOD (laser dose: 5 mJ/mm^2). Primary antibody: Anti-mCherry, Secondary: Alexa 488. Nuclear stain: DAPI (blue). (B) Reporter fluorescence intensity along lines drawn across the transfected cells. (C) Quantitative comparison of mCherry expression in membrane and cytoplasm. Mean ± S. D. *p<0.05.

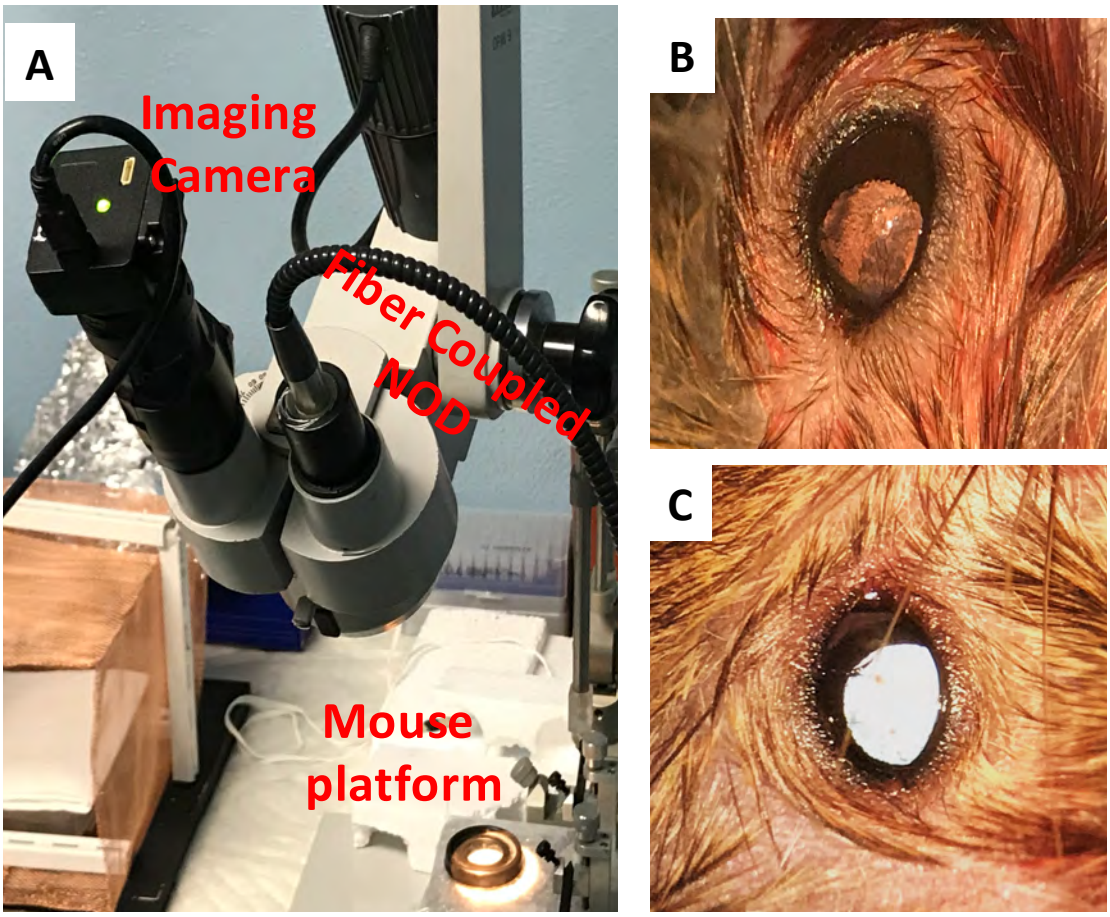

Suppl. Fig. 5. Set up for *in-vivo* NOD using 1064 nm continuous wave laser beam. (A) Picture of the set up, showing fiber-coupled laser beam and imaging camera integrated with a surgical microscope. (B) Image of mouse eye dilated with Tropicamide to allow NOD laser beam irradiation of retina. (C) Image of mouse retina being irradiated by the near-infrared NOD laser beam.

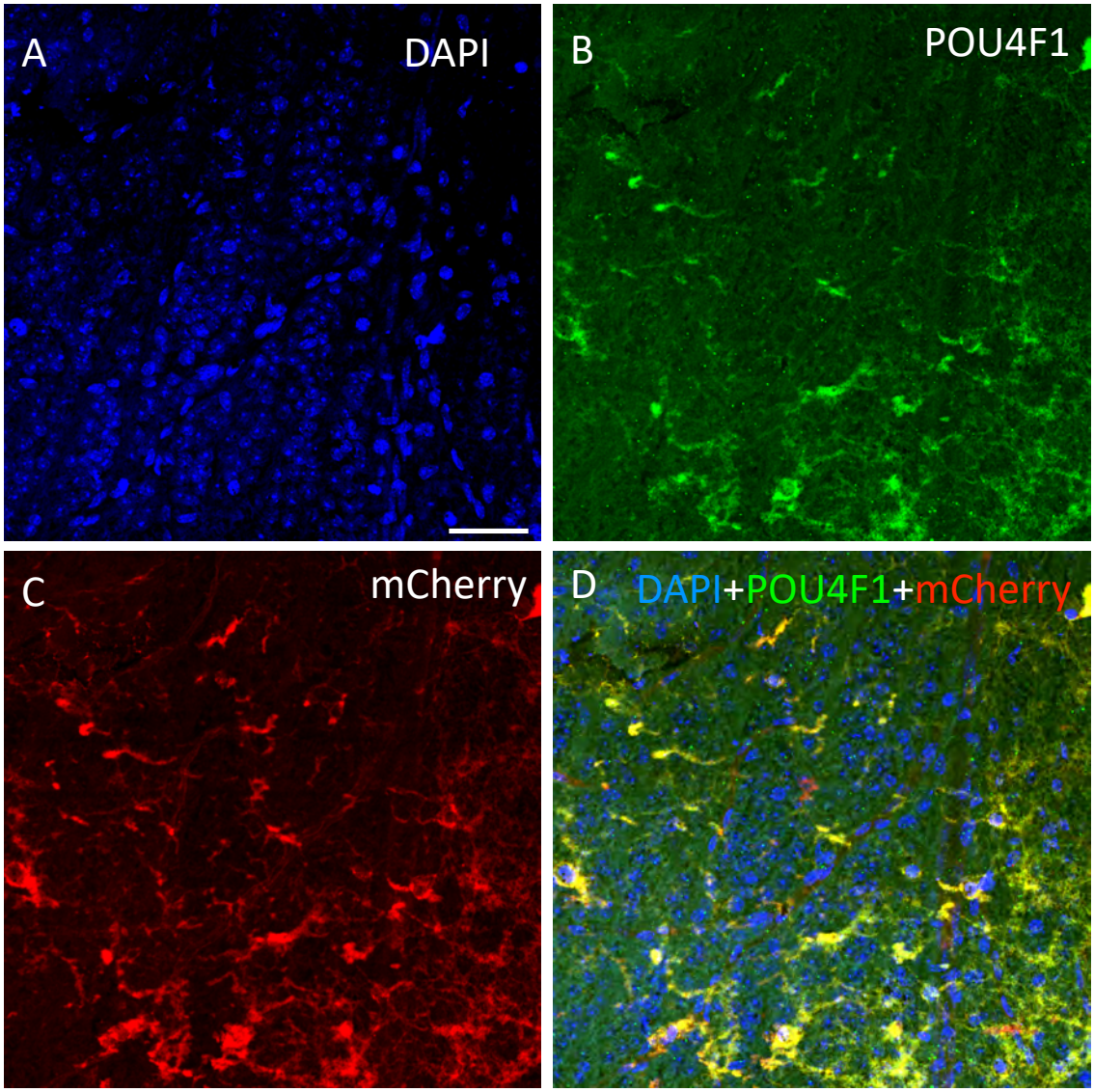

Suppl. Fig. 6. *In-vivo* optical delivery of MCO-II to *rd10* mice retina is Retinal Ganglion Cell specific. Fluorescence image of retina stained with: (A) nuclear stain DAPI. (B) RGC-specific staining using POU4F1. (C) Fluorescence image of reporter-mCherry expressed in retina after *in-vivo* optical delivery using CW 1064 nm laser beam. (D) Composite image of DAPI (blue), POU4F1 (green) and mCherry (red), showing co-localization of RGC with mCherry expression (yellow color). Scale bar = 50 µm.

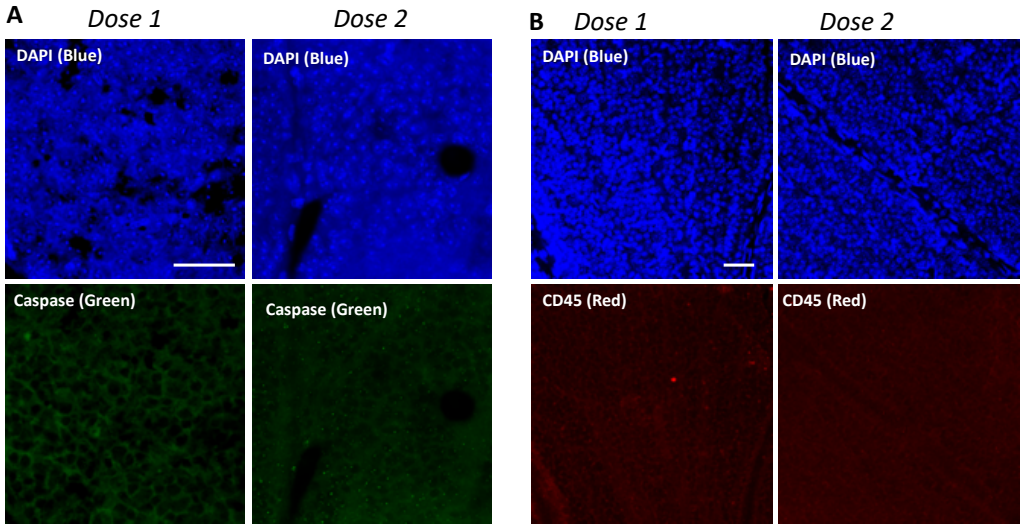

Suppl. Fig. 7. *In-vivo* optical delivery of MCO-II to *rd10* mice retina does not compromise viability of retina or elicit immune response. (A) Representative fluorescence images of retina stained with Caspase-3 (green) and DAPI (blue) for two different cw laser doses. Dose 1: 1.8 J/mm^2 (30 mW for 60 s); Dose 2: 3.6 J/mm^2 (60 mW for 60 s). Non-detectable apoptotic cells after optical delivery. (B) No detectable CD45 (red) signal, suggesting the absence of immune cells after MCO transfection. Dose 1: 0.9 J/mm^2 (30 mW for 30 s); Dose 2: 1.8 J/mm^2 (30 mW for 60 s). Laser irradiation area: 1 mm^2. Scale bar = 50 µm.